Available online at www.sciencedirect.com
ScienceDirect
Journal of Power Sources 162 (2006) 1130–1136
JOURNAL OF POWER SOURCES
www.elsevier.com/locate/jpowsour

Water transport in the proton exchange-membrane fuel cell: Comparison of model computation and measurements of effective drag

Toshiaki Murahashi *, Masao Naiki, Enju Nishiyama

Department of Electrical and Electronic Engineering, Fukui University of Technology, 3-6-1 Gakuen, Fukui 910-8505, Japan

Received 29 June 2006; received in revised form 22 July 2006; accepted 24 July 2006
Available online 7 September 2006

Abstract

Water transport through the membrane of a PEMFC was investigated by measurement of the net drag under various feed gas humidity. Measured data were compared with computed results obtained using a two-dimensional cell model. Considering the change in the gas content related to the flow configuration, the humidity of the supply gas, reaction rates, and the mass balance of each gas species were derived at five sections along the flow channels. By solving these mass balance equations, the water transport rates and current density distribution were obtained along the flow channels for various feed gas humidity. The results for net drag computed from the model show a similar tendency, but are slightly higher than the measured values. This suggests that there is a certain resistance related to water transport at the cathode membrane interface in association with water production. The cause of this water transport resistance is discussed.

Keywords: Proton exchange membrane fuel cell; Water transport; Water management; Net water drag; Capillary effect

1. Introduction

The proton exchange membrane fuel cell (PEMFC) has attracted a great deal of attention in the last decade as a promising candidate for a high-efficiency low-emission power source in both mobile and stationary applications. For mobile use, fuel cells are usually operated under a relatively high current density in order to achieve higher power density. For stationary use, fuels cell are usually operated under moderate current density, in order to achieve higher efficiency. However, there are still many problematic issues that must be overcome. One major problem is the water management of fuel cells. The operation of a state-of-the-art PEMFC requires careful water management. At low humidity, the proton exchange membrane and electrode assembly (MEA) lose water, which leads to a rapid increase in ohmic resistance. Conversely, if too much liquid water is present in the cell, the pores in the electrodes will be filled with water and the passage of reactant gases obstructed. In other words, the operating conditions and MEA components have to be well matched in order to avoid membrane dehydration and cathode flooding. In addition to the experimental approach, models for water management are useful to understand the processes that govern water transport. A clear understanding of water transport processes will assist the optimization of fuel cell operating conditions and relevant electrode structure.

Several experimental results have been reported in the literature for the water transport in proton exchange membranes (PEM), such as the net drag coefficients measured by Janssen et al. [1]. Although their investigation was mainly related to the effect of humidity, the humidity of the inlet gas was limited to a dry or wet condition. Ren et al. reported measurements for the electro-osmotic drag of water of a PEM in a direct methanol fuel cell (DMFC) [2]. The experiments were performed under the condition that the water flux across the membrane was exclusively driven by the electro-osmotic drag. Dong et al. reported current distribution, species distribution, and HFR (high frequency resistance) data, using a single serpentine flow channel in a co-flow arrangement, under mainly low-humidity conditions [3]. Experimental data suggest that humidification of the anode, rather than the cathode, was demonstrated as a most critical factor for achieving high performance at the inlet region.

It is useful that these experimental results are compared with computed results from a cell model. In addition to exper-

* Corresponding author. Tel.: +81 77 629 2549; fax: +81 77 629 7891.
E-mail address: murahasi@fukui-ut.ac.jp (T. Murahashi).

0378-7753/$ – see front matter © 2006 Elsevier B.V. All rights reserved.
doi:10.1016/j.jpowsour.2006.07.043

Nomenclature

a_j	activity of water in stream j (anode, cathode)
C	concentration of water in the membrane (mol cm^{-3})
D_w	diffusion coefficient of water (cm^2 s^{-1})
e	ratio of actual to apparent surface area
f_j	fraction j (solid s, open o) of porous surface
F	Faraday constant (96,485 C mol^{-1})
i_0	exchange current density (A cm^{-2})
I	local current density (A cm^{-2})
m	molar flow rate (along flow direction)(mol s^{-1} cm^{-2})
n_d	electro-osmotic drag coefficient
N_w	molar flux of water (perpendicular to the MEA) (mol s^{-1} cm^{-2})
p	pressure (kPa)
r	pore radius
R	gas constant (8.314 J mol^{-1} K^{-1})
S	surface area of the catalyst layer (cm^2)
t_d	dew point of feed gas (°C)
T	temperature (K)
V_o	open circuit voltage (V)
x	coordinate along the gas channel
y	coordinate perpendicular to the MEA

Greek symbols

α	net drag of water per proton
γ	surface tension
δ	thickness
ε	porosity of the electrode
η	over-potential for the ORR, V
ζ	stoichiometry
θ	contact angle
ρ	density of the catalyst layer
σ	conductivity of the membrane (Ω^{-1} cm^{-1})
τ	tortuosity factor

Subscripts

a	anode
c	cathode
in	inlet
m	membrane
out	exit
sat	saturation
v	vapor

imental investigation, much research has been performed for PEMFC modeling, which range from one-dimensional to three-dimensional models [4–11]. A one-dimensional model neglects the variation in the water content of the membrane, and the gas concentration along the flow channel. In order to investigate the distribution of gaseous species, the water content of the membrane, the current density and the net water transport along the flow channel, two-dimensional models have been developed. Nguyen et al. developed a combined heat and mass transfer model for a co-flow configuration under the condition that all of the water in the electrodes is in the vapor phase [7]. Janssen presented a two-phase, two-dimensional, along-the-channel model [8]. The model explains the water transport in electrodes under saturated and non-saturated gas conditions, by applying the concentrated solution theory under the assumption of uniform current density at all locations. During PEMFC operation with unsaturated reactant gases, especially at low stoichiometric flow rates, liquid water is likely to appear in the cathode. Pasaogullari and Wang modeled the two-phase flow and transport in the air cathode of a PEMFC, and concluded that capillary action is dominant inside the two-phase zone [9]. Recently, three-dimensional models have been developed to investigate the distribution of current density and temperature in the MEA and gas diffusion layer (GDL), and the distribution of gas velocity and gaseous species in the cross section of the GDL and flow channel under higher power density [10,11].

There have been few reports concerning the comparison of water net drag experimental results and computed simulation results. The purpose of the present work is to compare experimental net drag data, obtained under various reactant gas humidity and different operation modes, with the results computed using a relatively simple two-dimensional cell model.

2. Measurements of net drag

2.1. Experimental apparatus for net drag measurement

The change of water content in both the anode and the cathode flow channels was measured under various cell-operating conditions. A 25 cm^2 MEA was constructed using a Nafion112 membrane with a platinum loading of 0.5 mg cm^{-2} on both the anode and cathode. The MEA was mounted between two graphite current collector plates, each of which contained a serpentine channel machined to a width of 1 mm and a depth of 1.0 mm. The MEA was installed between two gaskets in order to prevent gas leakage. A counter flow configuration was used. Table 1 gives the specifications for the MEA.

The cell was operated at constant temperature, which was controlled by an electric heater. The feed gas humidity was controlled by bubbling of the gas through water that was maintained at a set-point temperature. At the exits of the gas flow channels, the water vapor was condensed in cold traps and the amount of water was measured at both the anode and the cathode. Before loading the platinum catalyst, a thin, hydrophobic, microporous layer was applied to the interface of the catalyst layer/GDL.

Table 1
Parameters used for the test cell

Parameter	Symbol	Value
Membrane equivalent weight	E	1200
Membrane thickness	δ_m	50×10^{-4} cm
Membrane dry density	ρ	1.84
Catalyst layer thickness	δ_{cat}	10×10^{-4} cm
GDL thickness	δ_{GDL}	300×10^{-4} cm
Tortousity factor	τ	5

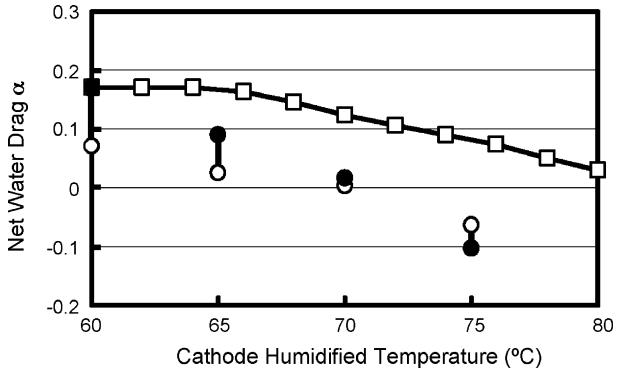

Fig. 1. Net water drag α, as a function of cathode humidified temperature (FC mode, $t_{cell} = 80\,^{\circ}C$, $t_{da} = 60\,^{\circ}C$, $\zeta_f = 1.43$, $\zeta_a = 2$); (□) calculation; (●, ◯) experimental results; (●) derived from the water balance at the cathode; (◯) derived from the water balance at the anode.

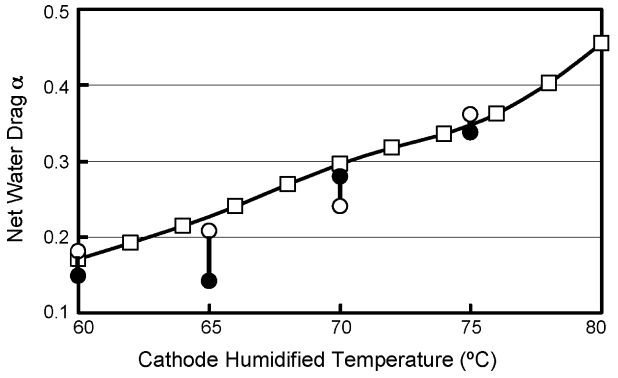

Fig. 2. Net water drag α, as a function of cathode humidified temperature (H_2 mode, $t_{cell} = 80\,^{\circ}C$, $t_{da} = t_{dc}$, $\zeta_f = 1.43$); (□) calculation; (●, ◯) experimental results; (●) derived from the water balance at the cathode; (◯) derived from the water balance at the anode.

In order to determine the water transport mechanism, two types of experiments (FC and H_2 mode) were performed. In H_2 mode operation, humidified hydrogen and nitrogen were supplied as anode and cathode feed gases, using the same bubbling water temperature, and a direct voltage was applied between the two electrodes. In this mode, no generation of water occurred at the cathode. Therefore, flooding in the GDL was not expected to have occurred in this operation mode. In the FC mode, humidified hydrogen and air were supplied as in conventional fuel cell operation. Measurements were conducted for 12 hours under each of the specified conditions.

2.2. Experimental results

Net water drag was derived from the measured water content for both FC and H_2 mode cell operating conditions at various feed gas humidity. The molar flux of water is given by the following equations for the cathode and anode, respectively:

$$N_{w,c} = \frac{I}{2F} + \alpha\frac{I}{F} \tag{1a}$$

$$N_{w,a} = \frac{\alpha I}{F} \tag{1b}$$

where the first term in Eq. (1a) is the flux of water generated in the cell reaction and the second term is that of net drag transport. Because the total molar flux of water are equivalent to the difference of water contents at the exit and inlet, the net drags are derived for the cathode and anode water contents, respectively:

$$\alpha = \frac{F}{I}(m_{H_2O,c,out} - m_{H_2O,c,in}) - \frac{1}{2} \tag{1c}$$

$$\alpha = \frac{F}{I}(m_{H_2O,a,in} - m_{H_2O,a,out}) \tag{1d}$$

At a current density of $0.3\,A\,cm^{-2}$, the stoichiometry at the anode and cathode are 1.43 and 2, respectively. The values of net drag are derived from the collected water weight at both the cathode and anode exits. The balance of the water collected at the anode and cathode was between 98.3 and 108.5% for various feed gas humidity. Figs. 1 and 2 show the net drag measured at a cell operating temperature of 80 °C during FC and H_2 mode operation, respectively. The range of each measured value indicates the difference between the anode and cathode data, derived from the change in the amount of water at the inlet and the exit. Computed results, based on the cell model, are also provided in these figures. The cell model is described in the following section.

For FC mode operation, the anode gas humidity was maintained at $t_{da} = 60\,^{\circ}C$, while the cathode gas humidity ranges between 60 and 75 °C. The humidity is expressed using the dew point of the inlet cathode (anode) gas as t_{dc} (t_{da}). The values of net drag decreased as the cathode gas humidity increased. For a humidity higher than $t_{dc} = 75\,^{\circ}C$, the net drag has negative values, which means water transfers from the cathode to the anode.

During H_2 mode operation, the humidity of the cathode gas was changed under the condition $t_{da} = t_{dc}$. Contrary to FC mode operation, the values of net drag increased as the humidity of the feed gas increased.

3. Discussion

3.1. Cell model

In order to evaluate the experimental results, a relatively simple two-dimensional cell model was developed. The schematic model is shown in Fig. 3. The model consists of a membrane

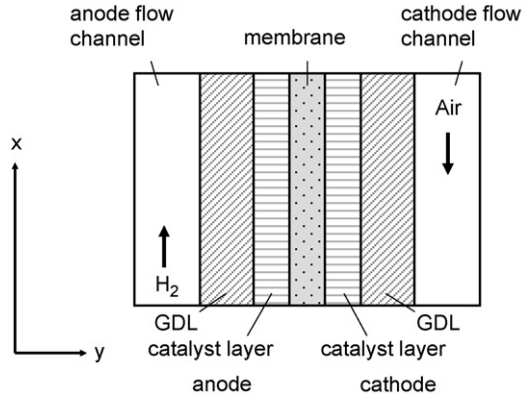

Fig. 3. Schematic model of PEMFC. x is a coordinate along the gas channel and y is a coordinate perpendicular to the membrane.

sandwiched between two gas diffusion electrodes (catalyst layers and gas diffusion layers) and two flow channels. The model accounts for the mass transport of water through the membrane (y-direction), the water content in the membrane and the current density distribution along the flow channel (x-direction). The baseline reactant gases of the anode and cathode are considered to be humidified hydrogen and humidified air or nitrogen, respectively.

3.1.1. Assumptions

In order to keep the water transport model simple, a number of assumptions are made:

1. The temperature is assumed to be uniform throughout the MEA and the flow channels. This assumption is rationalized for a small single cell maintained at constant temperature by an electrical heater.
2. An ideal gas mixture is assumed.
3. The water content in the membrane, at the interfaces of both electrodes is assumed to be in equilibrium with water vapor in the gases.
4. The pores of the catalyst layer and the GDL for gas diffusion are separated from the liquid flow passages. The existence of liquid water only modifies the effective porosity for gas diffusion.
5. The gases and liquid water are treated as being perfectly mixed and are assumed to flow with the same velocity.

3.1.2. Water transport

Water is transported in the membrane by electro-osmotic drag caused by proton transport and back diffusion due to the concentration gradient of water.

$$N_{\mathrm{w,a}} = n_{\mathrm{d}}\frac{I(x)}{F} - D_{\mathrm{w}}\frac{\partial C(x)}{\partial y} = \alpha\frac{I(x)}{F} \tag{2}$$

where α is the net drag coefficient.

The electro-osmotic drag coefficient (n_{d}) and the diffusion coefficient (D_{w}) are given by Springer et al. [4], using the activity of water, a_j, where j is applicable to both the anode (a) and the cathode (c) as follows:

$$\begin{aligned} n_{\mathrm{d}} &= 0.0049 + 2.024a_j - 4.53a_j^2 + 4.09a_j^3, \quad a_j \le 1 \\ &= 1.59 + 0.159(a_j - 1), \qquad\qquad\qquad\quad a_j > 1 \end{aligned} \tag{3}$$

$$a_j = C_j\frac{p}{p_{\mathrm{sat}}} \tag{4}$$

$$D_{\mathrm{w}} = n_{\mathrm{d}_j} \times 5.51 \times 10^{-7} \times \exp\left(2416 \times \left(\frac{1}{303} - \frac{1}{T}\right)\right) \tag{5}$$

3.1.3. Gas diffusion

Gas diffusion in the y-direction is expressed by the Stefan–Maxwell equation. In the cathode, the diffusion equation for the ternary gas mixture is simplified under the condition of flux $N_{\mathrm{N_2}} = 0$ ($\mathrm{N_2}$ is stagnant). In the anode, the diffusion equation for a binary gas mixture is applied. The following relationships exist between $N_{\mathrm{O_2}}$ and $N_{\mathrm{H_2O}}$ and current density I, in the cathode (direction of flux is defined from anode to cathode):

$$N_{\mathrm{O_2}}(x) = -\frac{I(x)}{4F} \tag{6}$$

$$N_{\mathrm{w,c}}(x) = \frac{I(x)}{2F}(1 + 2\alpha) \tag{7}$$

For a PEM electrode, $S\rho = 27.3 \times 10^4\ \mathrm{cm^{-1}}$ and $\varepsilon = 0.27$–0.35 are reported [12]. In the catalyst layer, micro carbon support particles aggregate to form the agglomerated structure, the peak diameter of which is approximately 0.07 μm, derived from an experimental pore distribution curve [12,13]. Since the mean free path of $\mathrm{H_2O}$ at 101.3 kPa is approximately 0.1 μm, it is reasonable to consider Knudsen diffusion. On the other hand, for the GDL, it is sufficient to consider only molecular diffusion, because the mean diameter of the GDL pores is approximately 30 μm. In an operating cell, the porosity of the cathode catalyst layer is expected to be less than that determined by BET (Brunner–Emmet–Teller) measurements, because a number of pores are filled with liquid water produced during the cell reaction. Assuming that $\varepsilon = 0.1$, the estimated $D_{\mathrm{eff,H_2O,O_2}}$, $D_{\mathrm{eff,O_2,N_2}}$ and $D_{\mathrm{eff,H_2O,H_2}}$ are 0.0043, 0.0033 and $0.0134\ \mathrm{cm^2\ s^{-1}}$, respectively, which is less than 1/60 of the molecular diffusion coefficients.

The effective diffusion distance in the direction of thickness is expressed as $\delta_{\mathrm{GDL}} \times \tau$, using the tortuosity factor (τ). Various values of the tortuosity factor, between 2.5 and 7, have been reported [1,14]. However, for the cell model, these values should be modified considering the cell configuration. Usually, in a PEMFC, reactant gases are supplied through gas channels that are constructed using machined carbon current collector plates adjacent to the GDL. Therefore, at the GDL/channel interface, there exists a channel section that contacts the reactant gas, and a collector section to which the reactant gas is not directly supplied. The reactant gases supplied from the channel section are transferred to the membrane/electrode interfaces, diffusing toward the rear of the collector section. The gas diffusion effect in the planar direction can be estimated by comparing the computed oxygen concentration at the GDL/catalyst layer using the two-dimensional (y–z-direction) diffusion equation, and that computed by the one-dimensional (y-direction) diffusion equation. The difference between these concentrations is equivalent to the difference between the effective diffusion distances. The increase in the effective diffusion distance is estimated to be approximately 15%. Based on an average of the reported tortuosity factors, and the increase in effective diffusion distance, a tortuosity factor of $\tau = 5$ is applied to the following computation.

3.1.4. Distribution of current density and water transport

The relationships shown in Eqs. (8)–(10) exist between the cell output voltage V, the current density I, the cell over potential η, and the membrane ion conductivity σ. The distribution of the current density along the flow channel is calculated using Eqs. (8)–(10) under the condition of a uniform cell voltage along the

flow channel and a given total current:

$$V = V_0 - \eta - \frac{\delta_m I(x)}{\sigma} \tag{8}$$

$$\sigma = (0.00514 \times 8.8 n_d - 0.00326) \times \exp\left(1267 \times \left(\frac{1}{303} - \frac{1}{T}\right)\right) \tag{9}$$

$$\eta = \frac{2RT}{F} \ln\left(\frac{I(x)}{i_0 p_{O_2}}\right) \tag{10}$$

In the cell model, the cell is divided into five sections in the x-direction. In each section, the mass balance of each gas species is expressed as a set of non-linear equations. These sets of equations are solved by the Newton method to obtain the distribution of current density, net water drag and the contents of gas species along the flow channel.

3.2. Comparison of the model computation and experimental measurements

3.2.1. Water drag dependence on humidification temperature

Comparison of the measured net drag with the computed results derived from the previously described cell model are shown in Figs. 1 and 2. Although the calculated results are slightly higher than the measured values, they do demonstrate the tendency well, especially for the H_2 mode. The discrepancy in the computed results from the FC mode is larger than that from the H_2 mode. This suggests that there is a resistance of some kind for the transport of generated water to the cathode channel at the cathode electrode/membrane interface.

The pressure of the water in the catalyst layer is higher than the saturation pressure, due to the existence of the hydrophobic microlayer at the cathode/membrane interface (capillary effect). This means that the activity of water at the cathode/membrane interface is increased by the existence of this hydrophobic microlayer. The pressure of the water is expressed in Eq. (11), using surface tension (γ), and apparent contact angle (θ).

$$p = p_{sat} - \frac{2\gamma}{r}\cos\theta \tag{11}$$

Apparent contact angle on a rough porous surface, such as a textile surface, is expressed using the true contact angle θ_t [16].

$$\cos\theta = f_s \cos\theta_t - f_o \tag{12}$$

where f_s and f_o are fractions of solid and open areas of the hydrophobic microlayer, respectively. If the true contact angle θ_t, is greater than 90°, the apparent contact angle θ, is increased. The apparent contact angle θ, is estimated to be between 150° and 160° (under the condition of a true contact angle range between 120° and 140°, and a solid fraction $f_s = 0.3$). The pressure of water in the catalyst layer is determined by the maximum pore size of the GDL. The increase of water pressure is estimated to be approximately 0.08 bar, using the surface tension $\gamma = 0.063\ \mathrm{N\,m^{-1}}$ and a pore radius $r = 30\ \mu\mathrm{m}$. A pore radius of $r = 30\ \mu\mathrm{m}$ is applied because the diameters of 90% of the pores in the GDL are in the range less than 60 μm. Net drags were computed again, substituting Eq. (11) for the partial pressure p, in Eq. (4). The results are shown in Fig. 4. The newly computed net water drags (solid squares) are approximately 0.02–0.07 lower than the corresponding previous data (empty squares). Although a discrepancy still exists, the coincidence between the experimental and computed data was improved. This suggests a contribution of capillary effect (suitability of hydrophobic effect) to the net drag.

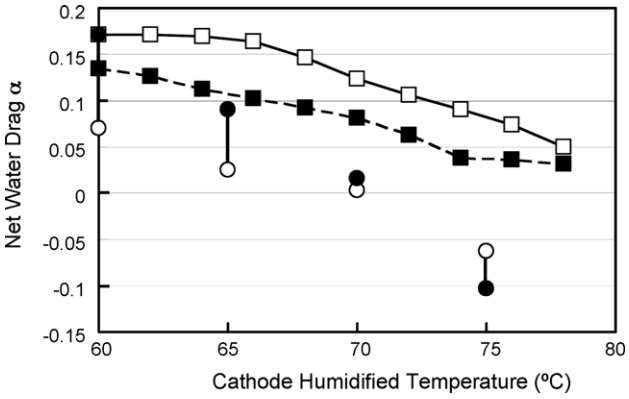

Fig. 4. Capillary effect on the net water drag α, as a function of cathode humidified temperature; (□) denotes the calculation without capillary effect and (■) denotes the calculation with capillary effect. (FC mode, $t_{cell} = 80\,^\circ\mathrm{C}$, $t_{da} = 60\,^\circ\mathrm{C}$, $\zeta_f = 1.43$, $\zeta_a = 2$); (●, ○) are the same as shown in Fig. 1.

The water content in the cathode gas increases along the flow channel by the accumulation of generated water and net water drag. Therefore, the water vapor in the cathode gas may reach saturation pressure at a downstream position. The net water drag depends on two factors given in Eq. (2), i.e. the electro-osmotic drag coefficient n_d, and the difference in activity between the cathode and the anode. Fig. 5 shows the net drag along the flow channel for various humidity of the inlet anode gas at relatively low cathode humidity, $t_{dc} = 64\,^\circ\mathrm{C}$, where the humidity t_{dc}, is expressed using the dew point of the inlet cathode gas. Fractional distance refers to the normalized distance from the inlet to the

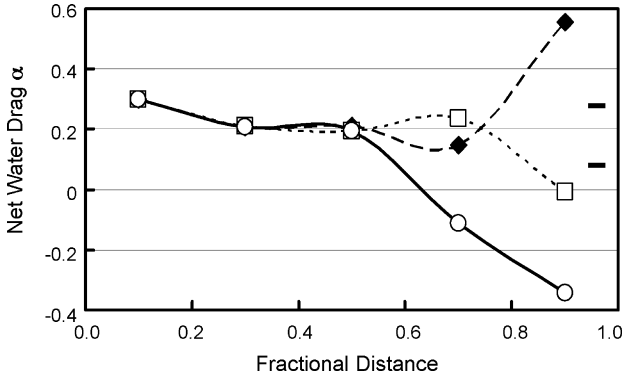

Fig. 5. Change of net water drag α, along a cathode flow channel for various humidity of the anode inlet ($t_{cell} = 70\,^\circ\mathrm{C}$, $t_{dc} = 62\,^\circ\mathrm{C}$). The horizontal axis is the fractional distance along the cathode flow channel. (♦) $t_{da} = 70\,^\circ\mathrm{C}$; (□) $t_{da} = 65\,^\circ\mathrm{C}$; (○) $t_{da} = 52\,^\circ\mathrm{C}$.

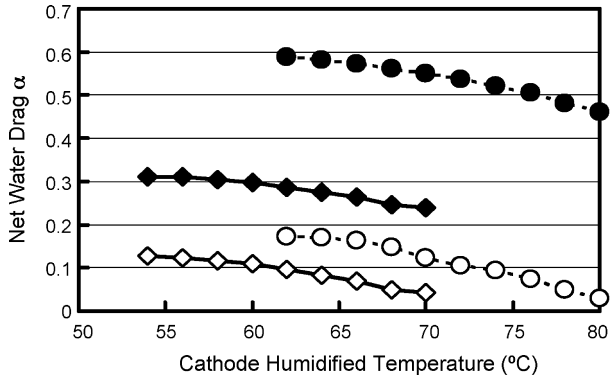

Fig. 6. Net water drag α, as a function of cathode humidified temperature. Parameters: (a) $t_{cell} = 80\,^{\circ}C$, $t_{da} = 80\,^{\circ}C$ (●), 60 °C(◯); (b) $t_{cell} = 70\,^{\circ}C$, $t_{da} = 70\,^{\circ}C$ (♦), 52 °C (◊).

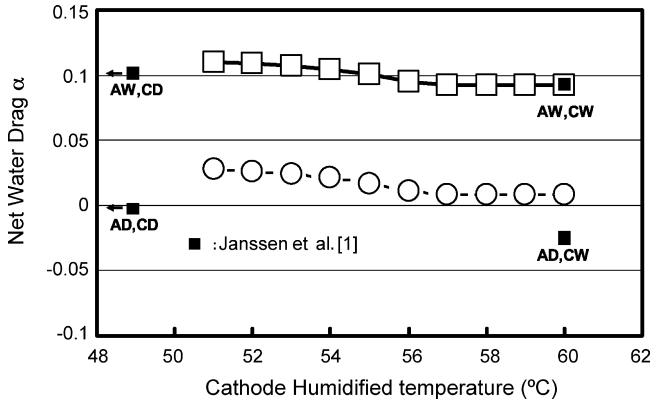

Fig. 7. Comparison of experimental data with computed results from the present model. Experimental data are from Janssen [1] and is marked as (■). The calculation was performed under the same conditions as described in [1]. Cell temperature and operating pressure are 60 °C and 1.5 bar, respectively. (□) $t_{da} = 60\,^{\circ}C$; (◯) $t_{da} = 32\,^{\circ}C$. AD and CW represent anode/dry and cathode/wet ($t_{dc} = 60\,^{\circ}C$)conditions, respectively.

exit. For most of the cell area from the cathode inlet, the net drags do not show any significant change for a wide range of inlet humidity. Near the cathode exit (between the normalized distance 0.7 and 0.9), the net drag is widely distributed, from 0.55 to −0.34, for a wet anode gas ($t_{da} = 70\,^{\circ}C$) to a dry anode gas ($t_{da} = 52\,^{\circ}C$). The average net drag ranges between 0.076 and 0.275, as shown by the dashed line in Fig. 5. This indicates that the change of net drag shown in Fig. 1 depends mainly on the humidity near the cathode exit.

In the previous experiments (Figs. 1 and 2), the net water drag was measured under a relatively low humidity anode gas condition. The net water drag for various humidity (t_{dc}) of the inlet cathode gas was calculated, and the results are shown in Fig. 6 for wet anode gas ($t_{da} = 80\,^{\circ}C$) and dry anode gas ($t_{da} = 60\,^{\circ}C$). For a wet anode gas condition, the value of net water drag is larger than that for a dry anode gas condition. However, the computed net drag for a wet anode gas and dry cathode gas condition is approximately 0.6, which is far less than the measured value of 1.0 at saturation [15]. This difference is due to back diffusion.

In order to compare the present model with the reported experimental results [1], computations for different fuel cell operation conditions were made. The conditions used for computation were as follows; current density 0.4 A cm^{-2}, pressure 1.5 bar, cell temperature 60 °C and stoichiometry of 1.5 and 2 for the anode and cathode, respectively. The humidity of the cathode is changed under two different anode humidity (wet and almost dry) conditions. The computed results are shown in Fig. 7, with the experimental data, and they are in good agreement.

3.2.2. *Sustainability of operation under the dry condition*

When the cathode gas at the channel is dry, the flux of water vapor from the cathode electrode/membrane interface to the cathode gas channel may exceed the rate of water production and water transported from the anode. This eventually causes drying of the cathode catalyst layer and membrane. However, the performance of the fuel cell has been shown to be stable up to an operating cell temperature of 60 °C, even under a dry air condition [17].

This result suggests the existence of a mechanism to maintain minimum water content in the membrane and the catalyst layer under dry gas conditions. A liquid–vapor water interface with a small meniscus exists in porous media. The pressure difference across the interface causes a change in the free energy, which is expressed by the following Kelvin equation [18]:

$$\frac{p_w}{p_{sat}} = \exp\left(-\frac{2\gamma}{rRT}\right) \tag{13}$$

where p_w is the vapor pressure above the meniscus, and p_{sat} is the vapor pressure at the free surface. This shows that the equilibrium vapor pressure of the meniscus decreases from that of the free surface. Under a dry or unsaturated gas condition, the water vapor pressure at the electrode/membrane interface is distributed along the flow direction, and is less than the saturation pressure for the cell temperature. Under the basic cell operation conditions ($t_{dc} = 65\,^{\circ}C$), the water vapor pressure at the electrode/membrane interface is distributed from 28.2 to 31.1 kPa and increases towards the exit, as shown in Fig. 8 (solid square). The difference in vapor pressure can be explained by the decrease in the equilibrium vapor pressure, as shown

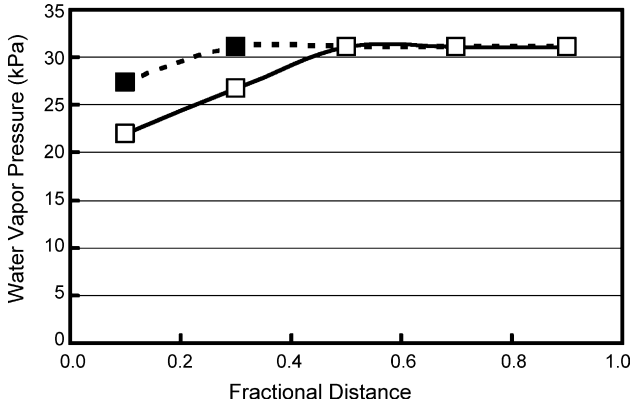

Fig. 8. Change of water vapor pressure along a cathode flow channel for different humidity of the cathode inlet ($t_{cell} = 70\,^{\circ}C$, $t_{da} = 65\,^{\circ}C$); (■) $t_{dc} = 65\,^{\circ}C$; (□) $t_{dc} = 60\,^{\circ}C$.

in Eq. (13). At a fractional distance of 0.1, pores smaller than 45.4 nm hold and keep water. For the lower humidity condition ($t_{dc} = 60\,^{\circ}C$, open square), pores smaller than 14.1 nm hold and keep water. Although under dry and unsaturated gas conditions, liquid water contained in relatively large pores evaporates, liquid water still exists in micro pores and this explains the experimental data for stable cell performance observed even under dry conditions.

4. Conclusion

Net drag was measured for H_2 and FC mode operations under various humidity conditions. In contrast to FC mode operation, flooding in the cathode GDL is not expected to occur for H_2 mode operation. In addition to these measurements, a two-dimensional water transport model for a proton-exchange membrane fuel cell was developed. Net water transport from the anode to the cathode varies along the flow channel, depending on the net drag and current density distribution. The distribution of current density along the flow channel was calculated using the membrane ionic conductivity and over-potential under a condition of uniform cell voltage.

The measured net drag was compared with the results computed using the two-dimensional cell model. Although the calculated results are slightly higher than the measured values, they followed similar trends. However, there was a larger discrepancy for the FC mode operation, and this suggests that a resistance of some kind exists for water transport to the cathode channel from the cathode/electrode interface. The hydrophobic microlayer that is applied to the interface of the catalyst layer/GDL is considered to be one candidate for the resistance to water transport, and the effect on the net water drag was estimated.

Acknowledgment

This work was supported by Research and Development of Polymer Electrolyte Fuel Cells from the New Energy and Industrial Technology Development Organization (NEDO) of Japan.

References

[1] G.J.M. Janssen, M.L.J. Overvelde, J. Power Sources 101 (2001) 117.
[2] X. Ren, S. Gottesfeld, J. Electrochem. Soc. 148 (2001) A87.
[3] Q. Dong, M.M. Mench, S. Cleghorn, U. Beuscher, J. Electrochem. Soc. 152 (2005) A2114.
[4] T.E. Springer, T.A. Zawodzinski, S. Gottesfeld, in: R.E. White, M.W. Verbrugge, J.F. Stockel (Eds.), Modeling Water Content Effects in Polymer Electrolyte Fuel Cells, PV91-10, Electrochemical Society Softbound Proceeding Series, 1991, p. 209.
[5] T.E. Springer, M.S. Wilson, S. Gottesfeld, J. Electrochem. Soc. 140 (1993) 3513.
[6] D.M. Bernardi, M.W. Verbrugge, AIChE J. 37 (1991) 1151.
[7] T.V. Nguyen, R.E. White, J. Electrochem. Soc. 140 (1993) 2178.
[8] G.J.M. Janssen, J. Electrochem. Soc. 148 (2001) A1313.
[9] U. Pasaogullari, C.Y. Wang, J. Electrochem. Soc. 151 (2004) A399.
[10] S. Dutta, S. Shimpalee, J.W. Van Zee, J. Appl. Electrochem. 30 (2000) 135.
[11] S. Um, C.Y. Wang, J. Power Sources 125 (2004) 40.
[12] J. Ihonen, F. Jaouen, G. Lindbergh, A. Lundblad, G. Sundholm, J. Electrochem. Soc. 149 (2002) A448.
[13] M. Uchida, Y. Fukuoka, Y. Sugawara, N. Eda, A. Ohta, J. Electrochem. Soc. 143 (1996) 2245.
[14] H. Ju, C.Y. Wang, S. Cleghorn, U. Beusher, J. Electrochem. Soc. 152 (2005) A1645.
[15] T.A. Zawodzinski, J. Davey, J. Valerio, S. Gottesfeld, Electrochim. Acta 40 (1995) 297.
[16] A.D. Adamson, Physical Chemistry of Surfaces, Interscience Publishers, 1960, p. 358.
[17] F.N. Buchi, S. Srinivasan, J. Electrochem. Soc. 144 (1997) 2767.
[18] A.D. Adamson, Physical Chemistry of Surfaces, Interscience Publishers, 1960, p. 58.